Remaining Flying Time Prediction Implementing Battery Prognostics Framework for Electric UAV's

Chetan Kulkarni*
SGT, Inc. NASA Ames Research Center, Moffett Field, CA 94035, USA
Edward Hogge†
Northrop Grumman Technical Services, NASA Langley Research Center, Hampton, Virginia 23681, USA
Cuong C. Quach‡
NASA Langley Research Center, Hampton, Virginia 23681, USA

Abstract

In this paper the problem of building trust in the online safety prediction of an fixed wing small electric unmanned aerial vehicles (e-UAV) for remaining flying time is addressed. A series of flight tests are described to verify the performance of the remaining flying time prediction algorithm. The estimate of remaining flying time is used to activate an alarm when the predicted remaining time falls below a threshold of two minutes. This updates the pilot to transition to the landing sequence of the flight profile. A second alarm is activated when the battery state of charge (SOC) falls below a specified safety limit threshold. This SOC threshold is the point at which the battery energy reserve would no longer safely support enough aborted landing attempts. During the test flights, the motor system is operated with the same predefined timed airspeed profile for each test. To test the robustness of the developed prediction algorithm, partial tests were performed with and remaining were performed without a simulated power train fault. To simulate a partial power train fault in the e-UAV the pilot engages a resistor bank at a specified time during the test flight. The flying time prediction system is agnostic of the pilot's activation of the fault and must adapt to the vehicle's state. The time at which the limit threshold on battery SOC is reached, it is then used to measure the accuracy of the remaining flying time predictions. This is demonstrated through comparing results from two battery models being developed. Accuracy requirements for the alarms are considered and the results discussed.

I. Introduction

Improvements in battery storage capacity have made it possible for general aviation vehicle manufacturers to consider electrically-powered solutions. Currently a key obstacle to be overcome when considering adoption of electrical propulsion systems in e-UAV's is the development of trust in estimating accurately the remaining battery operating time based on loading conditions, usage, degradation etc. There are several ways in which predicting remaining operating time is more complicated for battery-powered vehicles than it is for vehicles with a conventionally-powered liquid-fueled combustion system. Unlike a liquid-fueled system, where the fuel tank's volume remains unchanged over successive refueling procedures, a battery's charge storage capacity will diminish over time as it ages. Another complicating feature of a battery system is the time-varying relationship between battery output power and current drawn. Whereas a conventional liquid combustion system uses an approximately constant amount of liquid fuel to produce a given motive power, the power from

*Intelligent Systems Division, Discovery and Systems Health Area, MS 269-3, Senior AIAA Member.
†Safety Critical Avionics Systems Branch, AIAA Member
‡Safety Critical Avionics Systems Branch

Figure 1. Edge 540 Vehicle

a battery system is equal to the product of battery voltage and current. Thus, as batteries are discharged, their voltages drop lower, and they will lose charge in a non-linear manner.

An electric unmanned aerial vehicle (e-UAV) was used in this study. The e-UAV is a 33% sub-scale version of the Zivko Aeronautics Inc. Edge 540T tandem seat aerobatic aircraft as seen in the Fig. 1. This vehicle has been actively used by researchers at NASA Langley Research Center to facilitate the rapid deployment and evaluation of Battery Health Management algorithms for electric aircraft since 2010.

Remaining flying time prediction algorithms focus on the prediction of battery charge depletion over a single e-UAV flight. A lower-bound on the battery state of charge (SOC) that is considered safe for flight is set at 30% in this work. Flying the vehicle with batteries below 30% SOC is considered to be a high-risk mode of operation. Policy and guidelines are set according to the rulings and the engineering judgment of the UAS Operations Office and the Aviation Safety Review Board. Such violations of operating guidelines are referred to here as a functional failure of the vehicle's mission.

The accuracy of onboard remaining flying time estimation algorithms is tested in this work. A series of controlled run-to-functional-failure flight experiments are conducted while a ground station operator monitors the battery health parameters. The pilot follows a flight plan of timed constant airspeed during the cruise leg of the flight profile path.

This paper describes results of flight tests done to assess the performance of an alarm that warns pilot and system operators when the estimated remaining flying time falls below a set SOC threshold for a decision to land the asset safely. The primary case scenario for remaining flying time predictions is to warn system operators when landing procedures must be initiated to avoid the aircraft motor batteries becoming too depleted and sustain from any further operation. Ground based tests of a typical missed approach maneuver were performed in a laboratory test facility. It was determined that initiating landing procedures when the e-UAV batteries reach 30% SOC would provide a sufficient energy buffer for at least two missed approach maneuvers without risk of exceeding battery current limits and the risk of excessive heating based upon ground tests. The predictive element to be tested in this work is an alarm that warns system operators when the powertrain batteries are within two minutes of reaching the 30% SOC threshold under current operating conditions. This should allow the pilot sufficient time to prepare for landing without exceeding a moderate work load. The performance requirements were defined and verified by repeating ground based run-to-functional-failure tests a specified number of times reported in.[1]

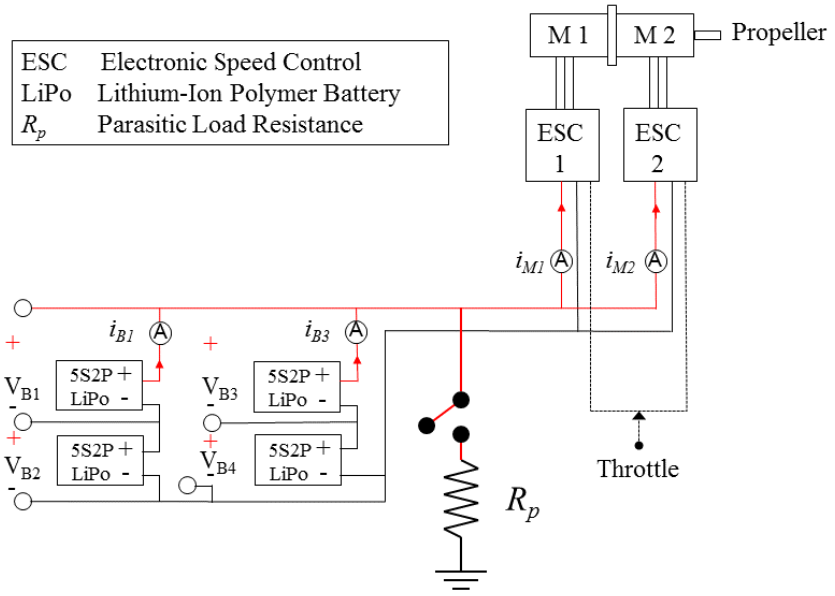

Figure 2. Schematic of electric Powertrain

II. Overview of the Edge 540 Electrical Powertrain System

A generic wiring diagram for the vehicle powertrain is shown in Fig.2. The aircraft has two 3-phase tandem motors that are mechanically coupled to the aircraft propeller. Powertrain batteries are arranged in two pairs of series connected battery packs. A switchable parasitic load R_p injects a fault to test the robustness of the remaining flying time estimation algorithms to changes in the battery loading demand.

Remaining flying time predictions are generated by propagating a number of estimates of the battery SOC forward. Forward propagation of the present battery state estimate is performed using an estimate of the future powertrain demand that will occur over the known flight plan. These future loads include propeller loads and parasitic loads. The prognostic tools make use of the known flight plan to inform future load predictions, but no prior information is assumed to be available regarding when a parasitic load may be injected.

Battery discharge prediction is described here in terms of the following components; (i) online battery state estimation; (ii) prediction of future battery power demand as a function of an aircraft flight plan; (iii) online estimation of additional parasitic battery loads; and (iv) prediction of battery discharge over the future flight plan.

III. Equivalent Circuit Model - Li- Ion Battery

The equivalent circuit model shown in Fig. 3 is used to replicate battery current and voltage dynamics as a function of estimated battery state of charge (SOC). This battery model contains six electrical components that are tuned to recreate the observed current-voltage dynamics of the Edge-540T battery packs. Battery charge is stored in the equivalent circuit model capacitor, C_b. The R_s, C_s and R_{cp}, C_{cp} circuit element pairs are used to capture standard battery phenomenon, such as internal resistance drops and hysteresis effects.

Since the equivalent circuit model is used to model the input-output response of a battery rather than its internal electrochemical states, the number of electrical components used, and there arrangement within an equivalent circuit vary depending upon the application. In addition, since battery input-output dynamics are known to change as a function of SOC, which is often the case that some of the parameters in an equivalent circuit model are parameterized as functions of battery state of charge (SOC).[2]

The following SOC parameterizations were used for the C_b, C_{cp}, and R_{cp} parameters in Fig. 3:

$$C_b = C_{Cb0} + C_{Cb1} \cdot \mathrm{SOC} + C_{Cb2} \cdot \mathrm{SOC}^2 + C_{Cb3} \cdot \mathrm{SOC}^3 \tag{1}$$

$$C_{cp} = C_{cp0} + C_{cp1} \cdot \exp\left(C_{cp2}\left(\text{SOC}\right)\right) \tag{2}$$

$$R_{cp} = R_{cp0} + R_{cp1} \cdot \exp\left(R_{cp2}\left(\text{SOC}\right)\right) \tag{3}$$

where the coefficients in the parameterized models for C_b, C_{cp}, and R_{cp} must be tuned based on observed current-voltage battery data over a range of battery SOC values.

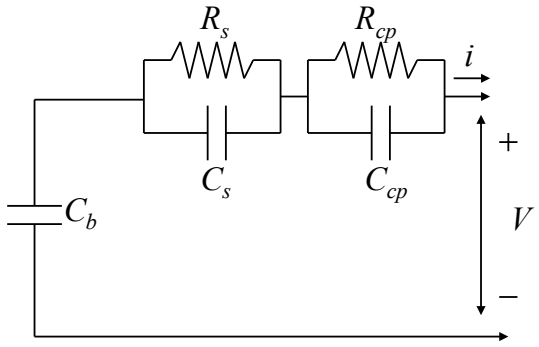

Figure 3. Equivalent circuit battery model.

Battery SOC is defined here as:

$$\text{SOC} = 1 - \frac{q_{max} - q_b}{C_{max}} \tag{4}$$

where q_b represents the charge stored in C_b, q_{max} is the maximum charge that the battery can hold, and C_{max} is the maximum charge that can be drawn from the battery. Note that, the maximum charge that can be drawn from the battery will be lower than the amount of charge stored in the battery due to electrochemical side-reactions that lock some portion of charge carriers in the battery. The term coulombic efficiency (CE) is used to refer to the portion of stored charge that is recoverable during the discharge of the battery. There are some mechanisms including resting the battery that can unlock some of its lost capacity, however, the overall trend is inevitably downward.

Data from laboratory experiments was used to fit all of the parameters in the equivalent circuit model to the lithium battery packs used on the Edge-540T. Adapting the equivalent circuit model to account for manufacturing variation and differences in battery state-of-health (SOH) is performed by varying only the battery charge storage capacity term, q_{max}, and the series resistance term, R_s, in equivalent circuit model. All other fitted parameters in the equivalent circuit model are constant across all Edge-540T packs. The q_{max} and R_s terms are identified by running separate characterization cycles for each battery pack prior to flight tests.

A test case example of measured and modeled battery voltage curves for laboratory characterization cycles are shown in Figs. 4 and 5. The results shown in Fig. 4 demonstrate a characterization experiment in which a battery is discharged at a low current of 0.044A (equivalent to an open circuit voltage) from a fully charged state. During this low current discharge test, the voltage across the C_b capacitor plays a dominate role. Thus, this experiment allows the C_b parameters in the equivalent circuit model to be fit in isolation.

Fig. 5 shows sample results from a second characterization experiment in which a battery is discharged using a series of current pulses. This experiment exposes voltage dynamics that must be fit by the R_s, C_s, C_{cp} and R_{cp} parameters in the equivalent circuit model.

A. Battery State Estimation

The identified battery model can then be used to implement an observer for the internal battery states based on sampled voltage and current data. The observer will attempt to estimate the internal states of each of the capacitors (C_b ,C_s, and C_{cp}) in the equivalent circuit model.

The unscented Kalman filter (UKF)[3,4] is a flexible tool for computing probabilistic belief in system state estimates based on stochastic (and possibly nonlinear) models of system dynamics. The UKF assumes a

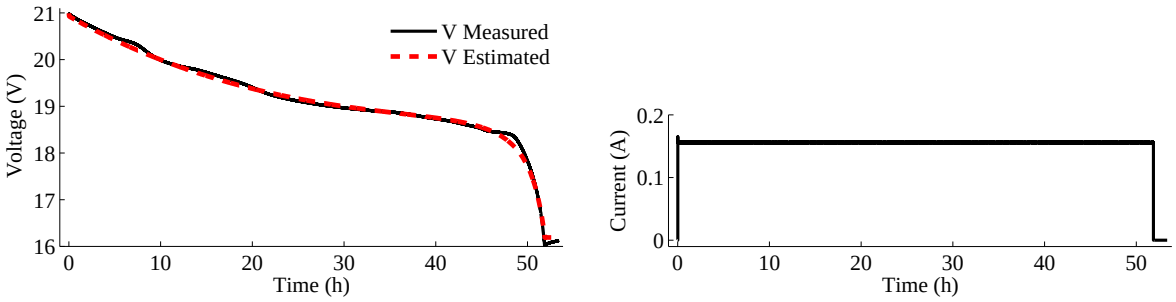

Figure 4. Comparison between measured and predicted battery voltage over a low current discharge.

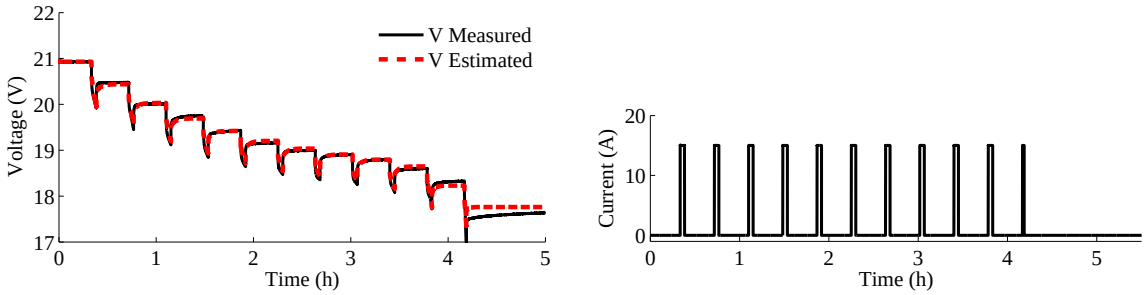

Figure 5. Comparison between measured and predicted battery voltage over a pulsed current discharge.

general nonlinear form of the state and output equations, and efficiently propagates model and state uncertainties without the need to calculate Jacobians (unlike the extended Kalman filter). The UKF is restricted to additive Gaussian noise random processes; however use of the unscented transform, a deterministic sampling method, allows random variables with non-Gaussian distributions to be incorporated using a minimal set of weighted samples, called *sigma points*.[3]

The UKF takes as inputs the system inputs, $\mathbf{u}(k)$, and the measured system outputs, $\mathbf{y}(k)$. The UKF gives as output, performing estimation using the battery model, a probability distribution for the state, $p(\mathbf{x}(k)|\mathbf{y}(0:k))$, described in the form of weighted sigma points $(\boldsymbol{\mathcal{X}}, \mathbf{w})$. From the sigma points, estimates of SOC, and voltage can be directly derived to obtain probability distributions of these quantities. The number of sigma points needed is linear in the dimension of the random variable, and so the statistics of the transformed random variable, i.e., mean and covariance, can be computed much more efficiently than by random sampling.[5]

IV. Electrochemistry Model - Li-Ion Battery

The electrochemistry model presented in[6] is based on the underlying electrochemical equations, but at a level of abstraction high enough that the model is still efficient with the improved fidelity. The model is represented as a set of ODEs and can be converted to a discrete-time representation and solved efficiently with a sample time of 1 s. Details of the developed model as discussed in .[6]

The battery model computes the voltage as a function of time given the current drawn from the battery. Several electrochemical processes contribute to the cell's potential. The different potentials are summarized in Fig. 6 (adapted from[7]). The overall battery voltage $V(t)$ is the difference between the potential at the positive current collector, $\phi_s(0,t)$, and the negative current collector, $\phi_s(L,t)$, minus resistance losses at the current collector.

The potentials at the current collectors are described by several voltage terms. At the positive current collector is the equilibrium potential $V_{U,p}$. This voltage is then reduced by $V_{s,p}$, due to the solid-phase ohmic resistance, and $V_{\eta,p}$, the surface overpotential. The electrolyte ohmic resistance then causes another drop

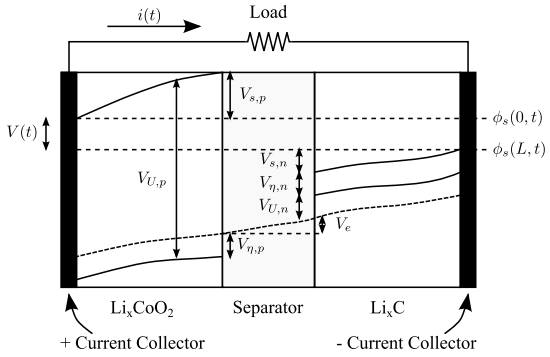

Figure 6. Battery voltages.

V_e. At the negative electrode, there is a drop $V_{\eta,n}$ due to the surface overpotential, and a drop $V_{s,n}$ due to the solid-phase resistance. The voltage drops again due to the equilibrium potential at the negative current collector $V_{U,n}$. The details of the battery modeling terms are discussed in [6]

A. Battery Voltage

Battery voltage can now be expressed as follows:

$$V = V_{U,p} - V_{U,n} - V'_o - V'_{\eta,p} - V'_{\eta,n}, \tag{5}$$

where

$$\dot{V}'_o = (V_o - V'_o)/\tau_o \tag{6}$$
$$\dot{V}'_{\eta,p} = (V_{\eta,p} - V'_{\eta,p})/\tau_{\eta,p} \tag{7}$$
$$\dot{V}'_{\eta,n} = (V_{\eta,n} - V'_{\eta,n})/\tau_{\eta,n}, \tag{8}$$

and the τ parameters are empirical time constants (used since the voltages do not change instantaneously).

The model contains as states $\mathbf{x}$, $q_{s,p}$, $q_{b,p}$, $q_{b,n}$, $q_{s,n}$, V'_o, $V'_{\eta,p}$, and $V'_{\eta,n}$. The single model output is V.

B. State of Charge

The state of charge (SOC) of a battery is defined to be 1 when the battery is fully charged and 0 when the battery is fully discharged by convention. In this model, it is analogous to the mole fraction x_n, but scaled from 0 to 1. We distinguish here between nominal SOC and *apparent* SOC.[6] Nominal SOC is computed based on the combination of the bulk and surface layer CVs in the negative electrode, whereas apparent SOC is be computed based only on the surface layer. When a battery reaches the voltage cutoff, apparent SOC is 0, and nominal SOC is greater than 0 (how much greater depends on the difference between the diffusion rate and the current drawn). Once the concentration gradient settles out, the surface layer will be partially replenished and apparent SOC will rise while nominal SOC remains the same. Nominal (n) and apparent (a) SOC are defined using

$$SOC_n = \frac{q_n}{0.6q^{\max}} \tag{9}$$
$$SOC_a = \frac{q_{s,n}}{0.6q^{\max_{s,n}}}, \tag{10}$$

where $q^{\max_{s,n}} = q^{\max}\frac{v_{s,n}}{v_n}$.[a]

C. Model Validation

Measured and predicted voltage curves for a 0.044 A discharge (approximately equal to open-circuit voltage) are shown in Fig. 7, and for a 2 A discharge in Fig. 8.

[a]Note that SOC of 1 corresponds to the point where $q_n = 0.6q^{\max_{s,n}}$, since the mole fraction at the positive electrode cannot go below 0.4, as described earlier.

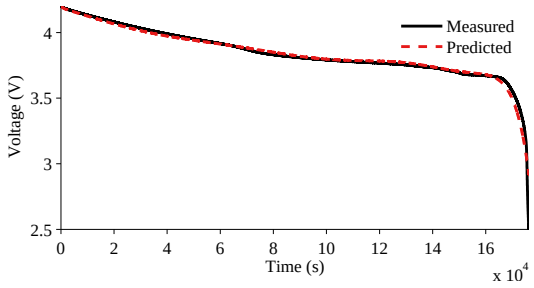

Figure 7. Comparison of predicted and measured open-circuit voltage.

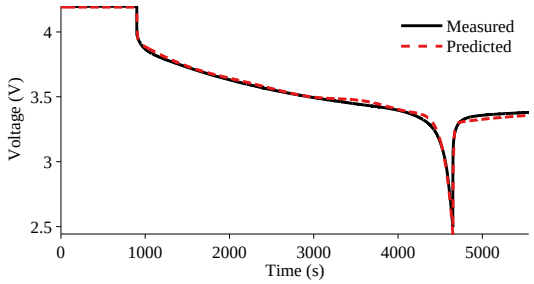

Figure 8. Comparison of predicted and measured voltage for a constant 2 A discharge.

V. Performance Requirements

The specification of performance requirements for ground verification of remaining flying time predictions is described next. The predictive element to be tested in this work is an alarm that warns system operators when the powertrain batteries are two minutes from reaching 30% SOC under normal operations. Accuracy requirements for the two minute warning are developed based on work by Saxena et al.[8]

1. The prognostic algorithm shall raise an alarm no later than two minutes before the lowest battery SOC estimate falls below 30% for at least 90% of verification trial runs.

2. The prognostic algorithm shall raise an alarm no earlier than three minutes before the lowest battery SOC estimate falls below 30% for at least 90% of verification trial runs.

3. Verification trial statistics must be computed using at least 20 experimental runs

4. At the end of the 2 minute warning period the pilot must have an option of doing 2 go arounds before the aircraft must land.

5. After the 2 minute warning it is advisable that the pilot not gain altitude.

6. The ending SOC estimation error as identified from the resting battery voltage must be less than 5% for at least 90% of verification trial runs.

Requirement one, the late alarm prediction bound, the alarm (two minute) is biased to occur early rather than late since the landing becomes unsafe if not enough charge reserve is present. Requirement two, the early alarm prediction bound, (three minute) limits the opportunity cost of unnecessarily denied flying time. Requirement three is an attempt to define a number to use to calculate quantified confidence limits. Requirement four is an energy reserve safety requirement to allow repeated landing attempts before battery exhaustion. Requirement five is a constraint on unplanned maneuvers close to the 30% SOC minimum energy for landing state to insure prognostic estimates for decision making will be reliable. Requirement six is an accuracy constraint on the diagnosis of the battery charge state.

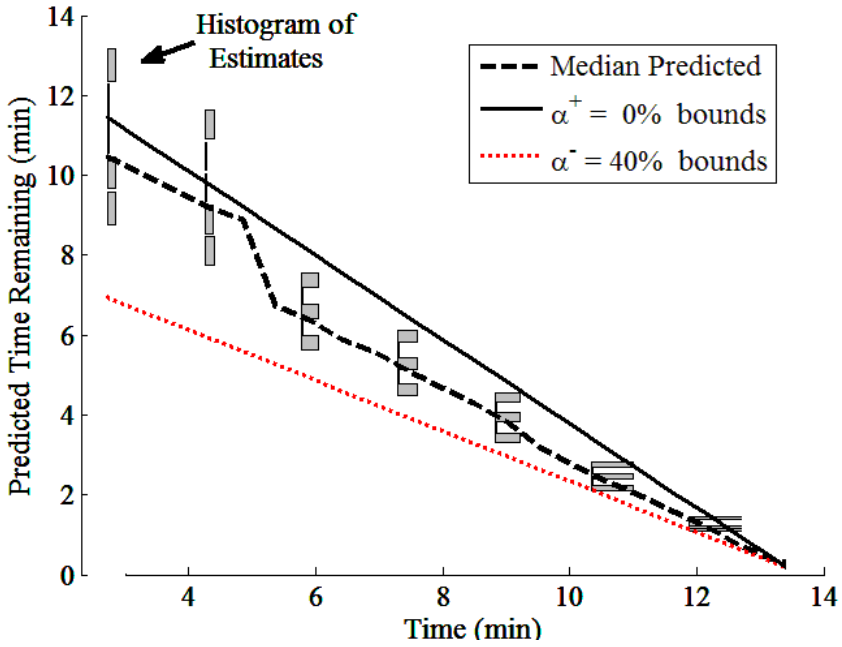

Figure 9. Histograms of predictions of flying time remaining within limit boundaries

The requirement definitions above use the term SOC estimate, because the UKF state estimation algorithm, relies upon to provide online estimates of battery SOC from measured battery current and voltages. A more direct measurement of battery SOC can be obtained after the experimental run is complete by allowing the batteries to rest until the terminal voltage settles to a constant value. There is a stable, empirical, relationship between resting battery voltage and SOC that can then be used to compute the ending SOC error of the powertrain batteries. The difference between the estimated battery SOC at the end of each experimental run and the measurement of SOC computed from the resting battery voltage is referred to as the SOC estimation error.

VI. Prediction of Battery Discharge Over a Flight Plan

The Prognostic Horizon metric defined by[9] is the difference in the time when the prediction meets error criteria and the time when the event predicted occurs. It is represented by the symbol λ. The accuracy of that prediction falls within a specified error margin denoted by the parameter α. The α margin limits are set according to the risk of early prediction and according to the risk of late prediction of the remaining flying time. In our case, the risk posed by late prediction of the time of zero remaining flying time is risk to the vehicle successfully landing. The risk posed by an excessively early prediction is the opportunity cost posed by landing too early and any additional missions needed to accomplish what was missed by landing early. The tuning of the estimation algorithm biases the prediction of remaining flying time to regard overestimation as a hazardous mode of operation to be avoided.[9] Ground Truth from a set of test flights was used to determine the actual remaining flying time on average, and the margin set to be the same (0%). Since the typical prediction accuracy fell between $\pm$20% error, the early prediction bound was set to 40% to bias the acceptable predictions to be early rather than late. This is reflected in the limit bound having a value of 0% indicating no tolerance for overestimation of remaining flying time. The limit bound for underestimation of remaining flying time is set to 40% below the ground truth value.

Fig.9 shows predictions of remaining flying time for the example run. The dark line in Fig. 9 denoted in the legend as indicates the true flying time remaining. The dashed line in Fig. 9 represents the median prediction of flying time remaining. The vertical extent of the histograms represents the interval between the minimum, median and maximum remaining flying time predictions. Here, the predicted

VII. Metric Prediction Performance

Prognostic algorithms inherently contain uncertainties and often estimate the uncertainties in the predicted quantity. These estimates can be used to infer the variability (spread) in predictions. In this section we discuss the metrics performance for around 10 flights on the Edge UAV and compare the results using the Equivalent Circuit Model as well as the Electrochemistry Battery Model. We calculate the SOC Ground Truth discuss the SOC Performance Results and Performance of Predicted Flying Time Warning.

VIII. Conclusion

The paper concludes with discussions from the results observed from both the models and future work.

References

[1]Hogge, E., Bole, B., Vazquez, S., Celaya, J., Strom, T., Hill, B., Smalling, K., Weber, and Quach, C., "Verification of a Remaining Flying Time Prediction System for Small Electric Aircraft," *Annual Conference of the Prognostics and Health Management Society 2015. Annual Conference of the Prognostics and Health Management Society 2015.*, 2015.

[2]Zhang, H. and Chow, M.-Y., "Comprehensive dynamic battery modeling for PHEV applications," *IEEE Power and Energy Society General Meeting*, 2010.

[3]Julier, S. J. and Uhlmann, J. K., "A new extension of the Kalman filter to nonlinear systems," *Proceedings of the 11th International Symposium on Aerospace/Defense Sensing, Simulation and Controls*, 1997, pp. 182–193.

[4]Julier, S. J. and Uhlmann, J. K., "Unscented filtering and nonlinear estimation," *Proceedings of the IEEE*, Vol. 92, No. 3, Mar 2004, pp. 401–422.

[5]Daigle, M., Saxena, A., and Goebel, K., "An Efficient Deterministic Approach to Model-based Prediction Uncertainty," *Annual Conference of the Prognostics and Health Management Society*, 2012.

[6]Daigle, M. and Kulkarni, C., "Electrochemistry-based Battery Modeling for Prognostics," *Annual Conference of the Prognostics and Health Management Society 2013*, Oct. 2013, pp. 249–261.

[7]Rahn, C. D. and Wang, C.-Y., *Battery Systems Engineering*, Wiley, 2013.

[8]Saxena, A., Roychoudhury, I., Celaya, J., Saha, S., Saha, B., and Goebel, K., "A Modeling Framework for Prognostic Decision Making and its Application to UAV Mission Planning," *AIAA Infotech Aerospace 2010*, 2010.

[9]*Metrics for Offline Evaluation of Prognostic Performance*, Vol. 1, 2010.